Molecular Cell
Article

Genome-Wide Identification of Fas/CD95 Alternative Splicing Regulators Reveals Links with Iron Homeostasis

J. Ramón Tejedor,[1,2] Panagiotis Papasaikas,[1,2] and Juan Valcárcel[1,2,3,*]
[1]Centre de Regulació Genòmica, Dr. Aiguader 88, 08003 Barcelona, Spain
[2]Universitat Pompeu Fabra, Dr. Aiguader 88, 08003 Barcelona, Spain
[3]Institució Catalana de Recerca i Estudis Avançats, Pg Lluis Companys, 23, 08003 Barcelona, Spain
*Correspondence: juan.valcarcel@crg.eu
http://dx.doi.org/10.1016/j.molcel.2014.10.029

SUMMARY

Alternative splicing of Fas/CD95 exon 6 generates either a membrane-bound receptor that promotes, or a soluble isoform that inhibits, apoptosis. Using an automatized genome-wide siRNA screening for alternative splicing regulators of endogenous transcripts in mammalian cells, we identified 200 genes whose knockdown modulates the ratio between Fas/CD95 isoforms. These include classical splicing regulators; core spliceosome components; and factors implicated in transcription and chromatin remodeling, RNA transport, intracellular signaling, and metabolic control. Coherent effects of genes involved in iron homeostasis and pharmacological modulation of iron levels revealed a link between intracellular iron and Fas/CD95 exon 6 inclusion. A splicing regulatory network linked iron levels with reduced activity of the Zinc-finger-containing splicing regulator SRSF7, and in vivo and in vitro assays revealed that iron inhibits SRSF7 RNA binding. Our results uncover numerous links between cellular pathways and RNA processing and a mechanism by which iron homeostasis can influence alternative splicing.

INTRODUCTION

Removal of introns from mRNA precursors (pre-mRNA splicing) is an essential step for the generation of functional mRNAs in eukaryotes. Alternative patterns of intron removal (alternative splicing [AS]) expand the coding potential of the genome and allow versatile regulation of gene expression in multicellular organisms. Most human transcripts undergo AS, thus representing an important mechanism for the generation of proteome diversity (Nilsen and Graveley, 2010). The process is tightly regulated to set up specific AS programs across different tissues or during development (Barbosa-Morais et al., 2012; Merkin et al., 2012).

The spliceosome, the complex machinery in charge of intron removal, is composed of >170 proteins and 5 snRNAs that help to recognize the boundaries between exons and introns. Spliceosome assembly proceeds in a stepwise manner through highly dynamic changes in protein composition and snRNA:pre-mRNA and snRNA:snRNA interactions (Wahl et al., 2009). Initial recognition of the 5′ and 3′ splice sites (ss) by U1 and U2 snRNP, respectively, is followed by the incorporation of the U5/4/6 tri-snRNP, which precedes the two sequential *trans*-esterification reactions leading to intron removal, which are believed to be catalyzed by snRNAs (Fica et al., 2013). Ss recognition can be modulated by additional splicing enhancer and silencer sequences located within introns and exons and recognized by splicing regulatory factors (Braunschweig et al., 2013; Fu and Ares, 2014). How these mechanisms are integrated with physiological regulation of AS and with the activity of other cellular pathways is only starting to be deciphered (Fu and Ares, 2014).

Genome-wide and high-throughput content screenings are emerging as powerful tools for the identification of regulators of a variety of cellular processes, including cell cycle progression, cell death, or cell transformation (Gazin et al., 2007; Chew et al., 2009; Neumann et al., 2010). Few genome-scale screens for the identification of splicing regulators in mammalian cells have been reported. Using a luciferase-based reporter minigene and a cDNA expression screen, Warzecha et al. (2009) identified ESRP1 and ESRP2 as epithelial-specific splicing regulators governing the splicing of the FGFR2 receptor. Using dual fluorescent reporters, a gain-of-function cDNA screen identified regulators of postsynaptic density protein 95 (Psd-95) AS (Zheng et al., 2013). Moore et al. (2010) employed fluorescent reporters to carry out a genome-scale siRNA screen to identify regulators of AS of the apoptotic genes BCL-X and MCL-1, establishing links between AS regulation and cell cycle progression. Despite their proved value, artificial reporter systems may fail to capture aspects of physiological regulation of AS, including those linked to the complex interplay between chromatin and splicing at endogenous gene loci or those affected by overexpression of fusion transcripts. Large content genome-wide screens based on endogenous transcript measurements have been technically challenging, and only one high-content mutational screen in yeast identified splicing regulators for endogenous target genes (Albulescu et al., 2012).

In this manuscript we report the results of a genome-wide siRNA screen for AS regulators of the endogenous Fas/CD95

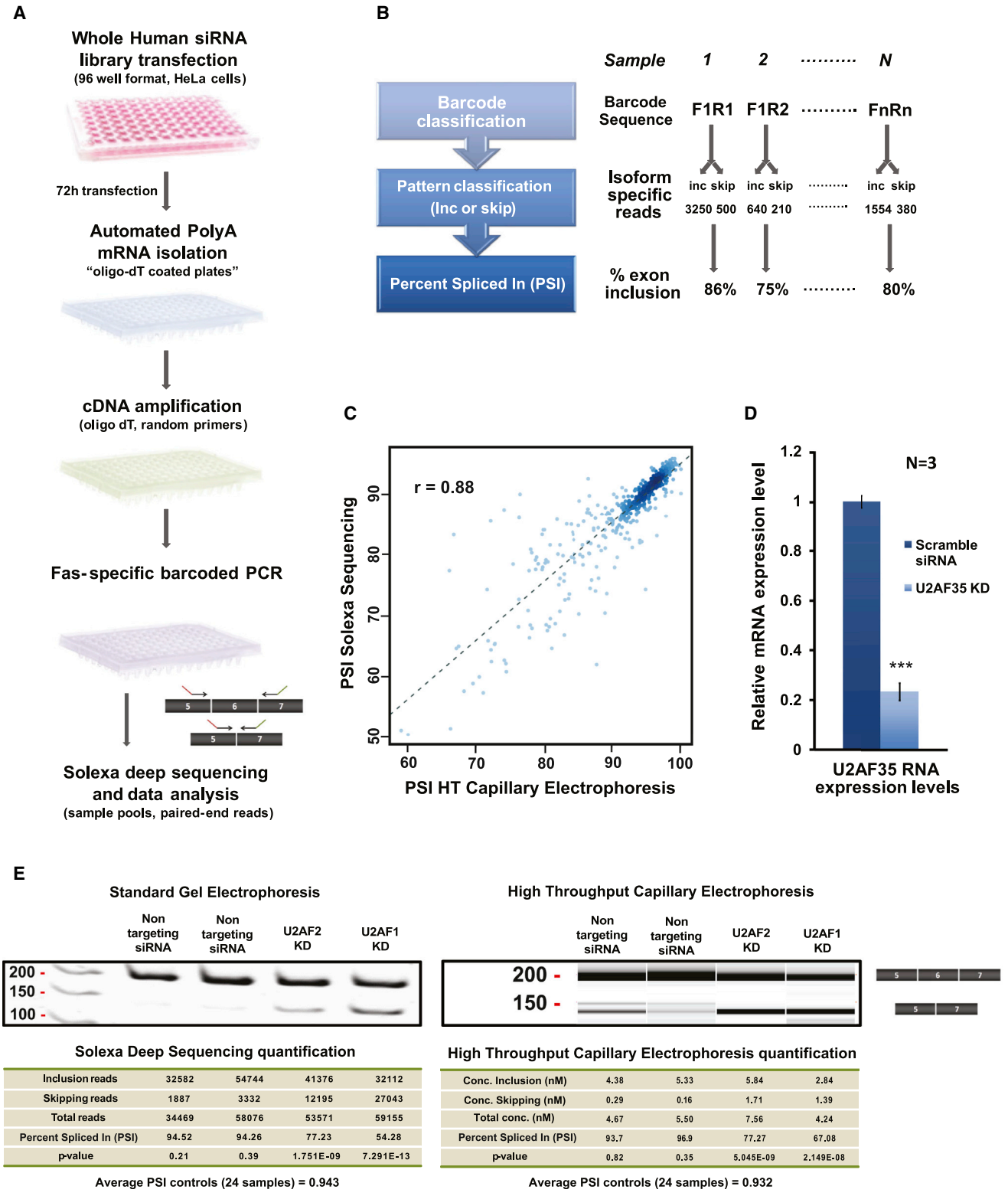

Figure 1. Genome-Wide Screening for Regulators of Fas/CD95 AS

(A) Scheme of the screening procedure.

(B) Barcode classification and isoform quantification pipeline. Deep sequencing reads were filtered based upon the barcode sequence combination, and the presence or absence of Fas/CD95 exon 6 sequences and the percentage of exon inclusion isoforms was calculated for each knockdown condition.

(legend continued on next page)

gene. Fas/CD95 encodes a cell surface death receptor that upon binding to the Fas Ligand leads to programmed cell death by activating the extrinsic apoptosis signaling pathway (Krammer, 2000). Interestingly, basal Fas/CD95 receptor activation was found to be required for stimulation of tumor growth in mouse cancer cells (Chen et al., 2010). AS contributes to the generation of different Fas/CD95 isoforms with opposing roles in apoptosis. Fas/CD95 exon 6 encodes a transmembrane domain, and skipping of this exon leads to an mRNA encoding a soluble form of the receptor that can act as a decoy and prevent cell death (Cheng et al., 1994; Cascino et al., 1995; Liu et al., 1995; Papoff et al., 1996). A switch in isoforms from soluble to membrane-bound occurs during T lymphocyte activation, and misregulation of this switch is associated with Autoimmune lymphoproliferative syndrome (ALPS) (Roesler et al., 2005).

By coupling automatized siRNA transfection, RNA isolation, and barcoded PCR amplification with deep sequencing quantification, we identified 200 factors involved in Fas/CD95 exon 6 AS regulation and revealed a connection between iron homeostasis and AS regulation in human cells. Combined with a functional splicing factor network analysis (see accompanying manuscript by Papasaikas et al., 2015), we identified the splicing factor SRSF7 (previously known as 9G8) as a mediator of iron-induced AS changes through iron-induced inactivation of its Zinc-knuckle RNA binding domain.

RESULTS

Genome-Wide siRNA Screen to Identify Regulators of Endogenous AS Events in Mammalian Cells

To systematically identify regulators of Fas/CD95 AS, a siRNA library (siGENOME, Dharmacon) comprising more than 22,000 pools of siRNAs targeting all known and predicted human protein-coding genes was transfected in HeLa cells using a robotized procedure (Supplemental Experimental Procedures available online). A total of 72 hr after transfection, mRNAs were isolated in oligodT plates using an automated protocol (Figure 1A), and cDNA libraries of the 22,000 transcriptomes were then generated by automatized reverse transcription using oligodT and random hexamers. To interrogate the ratio of Fas/CD95 exon 6 inclusion/skipping in these libraries, PCR reactions were set up using barcoded primers corresponding to sequences in the flanking exons 5 and 7. In this strategy, each individual siRNA condition is identified by a particular combination of two barcodes, one in each of the PCR primers (Figure 1A). To measure isoform ratios in each condition, the PCR products were pooled together (>26,000 different conditions including controls) and the sequences of individual molecules determined by paired-ended Illumina HiSeq sequencing (532 million reads in total, 100 nt length, obtained either from pooled or technical replicate samples) (see Supplemental Experimental Procedures). This provides on average more than 4,000 reads per technical replicate or 20,000 reads per knockdown condition, which allows a robust determination of isoform ratios (Tables S1 and S2). Data filtering allowed read classification based upon (a) the barcode combination and (b) the presence or absence of Fas/CD95 exon 6 sequences (Figure 1B; Supplemental Experimental Procedures). The Percent Spliced In (PSI) index (Katz et al., 2010) was determined as the ratio between exon 6-containing reads over the total number of reads in each condition, with changes in PSI even lower than 5% being reproducibly detected and validated.

The robustness of the screen was verified by comparing the PSI values for hundreds of replicas of control siRNAs and SLU7 (a known regulator of Fas/CD95 splicing) siRNAs (two-sided t test p value $< 1 \times 10^{-20}$) (Figures S1B and S1C). The accuracy of the deep sequencing method was validated by the following controls: (a) consistent PSI estimates were obtained by deep sequencing and high-throughput capillary electrophoresis (HTCE) over a dilution range of three orders of magnitude, for control samples containing defined ratios of Fas/CD95 inclusion and skipping isoforms (Table S1E); (b) a good correlation was observed between PSI values of biological replicas in a pilot screen focused on the knockdown of 250 splicing factors, estimated in parallel by both technologies (0.66 and 0.59, respectively) (Figures 1D, 1E, and S1A; Supplemental Experimental Procedures; Table S1); and (c) excellent correlation between PSI indexes estimated by the two technologies for 500 control samples from the genome-wide screen were also obtained (0.88 Pearson correlation) (Figure 1C), further validating the consistency of the screen results.

A total of 1,505 conditions were identified in which the knockdown of individual genes led to a statistically significant difference in PSI compared to the control siRNA pool ($-2 >$ Robust Z score $> +2$) (Figure 2A; Supplemental Experimental Procedures; Table S2). To further validate these results, biological triplicates of the knockdown hits were analyzed by HTCE, which enables the rapid separation and quantification of amplification products corresponding to the two isoforms for 96 samples in parallel. This resulted in 427 validated hits. The nonvalidated hits were usually closer to the cut-off (Figure S1) but may also reflect different sensitivities of the two technologies. As a second validation, and also to discard possible off-target effects of the siRNA pools, a second screen was carried out using siRNA pools from a nonoverlapping siRNA library against the 427 factors in biological triplicates. This resulted in 200 genes whose knockdown affects Fas/CD95 AS, validated with two independent siRNA libraries and two independent technologies (deep sequencing and HTCE, the latter in biological triplicates) (Figure 2B; Table S3).

(C) Correlation between percentage spliced in (PSI) values obtained by deep sequencing data and by HTCE for 500 control knockdown conditions.

(D) Example of mRNA knockdown validation. RNAs isolated from HeLa cells transfected with scrambled siRNAs or smartpool siRNA library siRNAs against U2AF35. Values represent the mean and SD from three biological replicas.

(E) Particular examples of comparative analysis, by three different technologies, of the effects on Fas/CD95 AS of knockdown of the two subunits of the splicing factor U2AF. Upper panels: results of semiquantitative RT-PCR, analyzed by standard gel electrophoresis (left) or HTCE (right). Lower panels: quantification of PSI values by Illumina HiSeq deep sequencing (left) or by HTCE (right). The factors knocked down and average PSI values of controls are indicated. See also Figure S1 and Table S1.

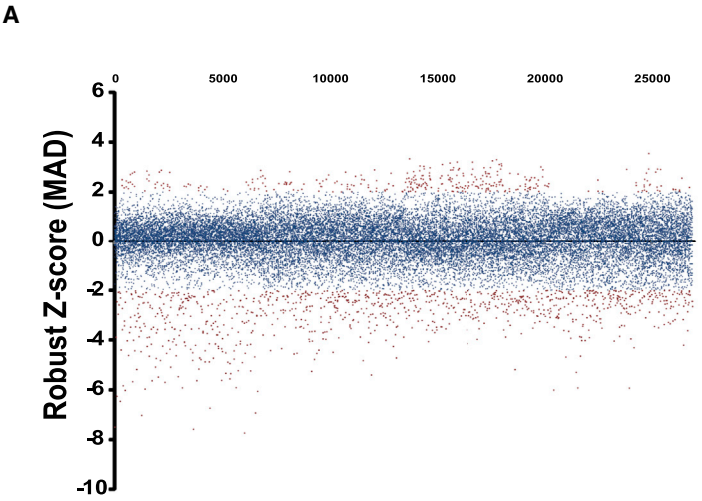

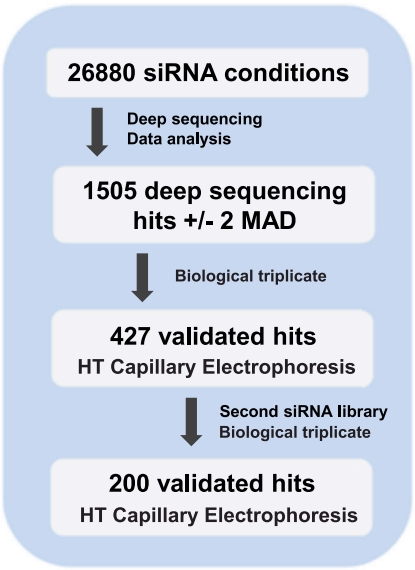

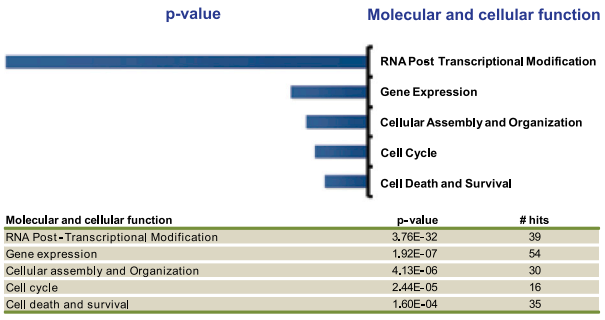

Molecular and cellular function	p-value	# hits
RNA Post-Transcriptional Modification	3.76E-32	39
Gene expression	1.92E-07	54
Cellular assembly and Organization	4.13E-06	30
Cell cycle	2.44E-05	16
Cell death and survival	1.60E-04	35

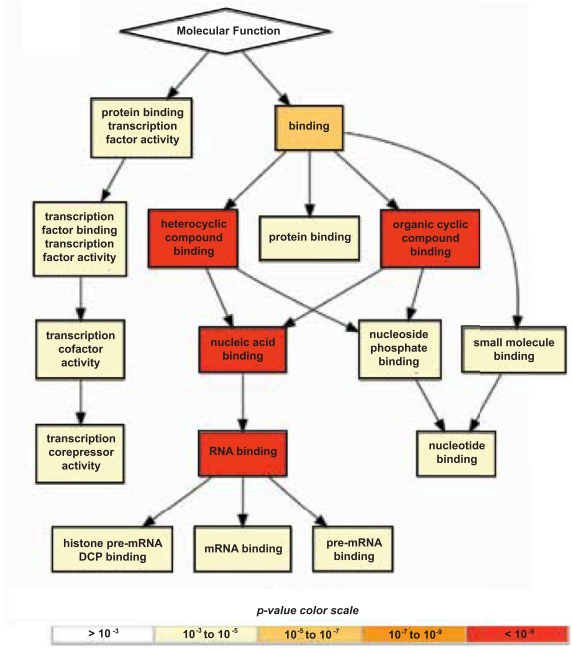

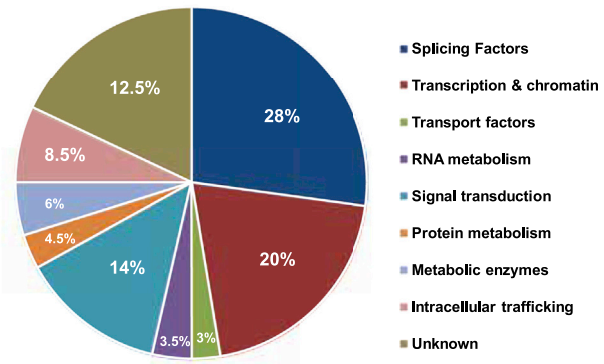

Figure 2. RNA Processing, Transcription, and Chromatin Factors Involved in Fas/CD95 AS Regulation

(A) Distribution of robust *Z* scores (see Supplemental Experimental Procedures) across the 26880 siRNA conditions analyzed. Screen hits with *Z* score values greater than +2 or below −2 are indicated in red.

(B) Flowchart of hit validation along the screening procedure. MAD indicates scaled median absolute deviation (see Supplemental Experimental Procedures).

(C) Functional GO terms enrichment for the fully validated 200 hits. The statistical significance of the enrichment (Ingenuity Pathway Analysis software) and the number of hits in each category are indicated.

(legend continued on next page)

Screening Hits Are Enriched in RNA Processing, Transcription, and Chromatin Factors

Functional gene ontology (GO) analysis of the validated 200 hits showed—as expected—a clear enrichment in RNA posttranscriptional modification factors. Other GO categories were also significantly enriched, including cell cycle and cell death (Figure 2C), suggesting possible links between Fas/CD95 AS and regulators of cell division and apoptosis. As expected, molecular functions related to nucleic acid/RNA binding were significantly enriched in the GO analysis (Figures 2D, S2A, and S2B). Interestingly, among the RNA processing factors identified, we observed an overrepresentation of core spliceosomal components and of factors acting late in spliceosome assembly over classical regulators of AS (Table 1; Table S3), suggesting extensive potential of the core splicing machinery for the modulation of ss choice. Additional results indicate that, under the conditions of our experiments, the knockdown of core splicing factors does not cause a generalized inhibition of splicing nor extensive cell death (see also accompanying manuscript by Papasaikas et al., 2015; Discussion).

Additional GO categories were also enriched (Table 2). A first category contains proteins involved in DNA metabolism, including transcription factors (e.g., MYC and MYBL1), proteins with dual roles in transcription and splicing that have been previously linked to DNA damage response (e.g., SKIIP or ZNF830), topoisomerase-associated factors (e.g., TOP2A and TOPB1), and chromatin remodeling factors (e.g., components of the SWI/SNF complex or the histone methyl-transferase SETD2). These factors may affect Fas/CD95 AS through mechanisms involving the coupling between transcription and RNA processing (reviewed by Kornblihtt et al., 2013; see Discussion). Factors involved in other aspects of RNA metabolism include components of the THO complex, which are deposited after capping and splicing of pre-mRNAs and promote RNA transport (Strässer et al., 2002), suggesting that differential export of transcript isoforms contributes to the observed ratios between alternatively spliced mRNAs. A third category of regulators of Fas/CD95 AS includes various factors acting outside of the nucleus to activate particular signaling pathways, including Fibroblast Growth Factor Receptor 1 (FGFR1) and several members of the Ras- and Rho- families of small GTPases. Particularly intriguing is the link between Fas/CD95 splicing and several genes encoding mitochondrial proteins involved in the regulation of energy metabolism, including enzymes implicated in sugar and fatty acid catabolism and oxidative phosphorylation (see Discussion).

Iron-Homeostasis-Related Genes Regulate Fas/CD95 AS

To gain further insights into connections between the spliceosome and other cellular pathways, we focused our attention on ACO1 and ferritin L chain (FTL), two genes with antagonistic roles in the control of iron homeostasis whose knockdown had opposite effects on Fas/CD95 AS. ACO1 encodes a moonlighting protein that functions, under conditions of iron abundance, as an enzyme that converts citrate to isocitrate and, upon iron-depletion, displays an RNA binding activity that modulates the stability/translation of target mRNAs encoding genes (like FTL) that control iron storage or uptake (Muckenthaler et al., 2003; Hentze et al., 2010). Under conditions of iron depletion, ACO1 represses FTL translation (Gray and Hentze, 1994), leading to the release of iron from ferritin storage sites. The results of the screen indicate that ACO1 depletion with two different siRNA pools (Figures 3A and S3C), which favors iron depletion (Figures 3B and S3A), promotes Fas/CD95 exon 6 skipping (Table 2, confirmed by capillary electrophoresis—Figure 3C—and by real-time PCR, which often provides more accurate values; Figure 3D). In contrast, FTL depletion with two different siRNA pools (Figures 3A and S3C), which favors iron release (Figures 3B and S3A), promotes exon 6 inclusion. Similar effects were observed using the hepatocellular carcinoma HepG2 cell line (Figures S3B and S3D).

Next, we explored the effects of pharmacological treatments that lead to intracellular iron overload (Hemin) or iron depletion (Desferal, Ciclopirox). As previously reported (Muckenthaler et al., 2003), Hemin treatment led to higher ferritin mRNA and protein levels, lower transferrin mRNA levels (Figures S3E and S3F), and an overall increase of intracellular iron (measured as a decrease in Phen-green SK fluorescence) in different cell lines (Figures 3B, S3A, and S3B). Conversely, treatment with Desferal had opposite effects (Figures 3B, S3A, and S3B). Consistent with the effects of ACO1/FTL depletion, iron excess induced by Hemin led to increased Fas/CD95 exon 6 inclusion, while iron depletion induced by Desferal or Ciclopirox increased exon 6 skipping, both in endogenous transcripts and in the context of transcripts expressed from a minigene reporter plasmid (Figures 3E and 3F). Taken together, these observations reveal a link between intracellular iron availability and differential regulation of Fas/CD95 alternatively spliced isoforms. While we cannot exclude effects of our screen hits on differential stability of the mRNA isoforms, similar half-lives for exon 6 inclusion and skipping transcripts were observed upon inhibition of transcription by Actinomycin D, including conditions of iron depletion or overload (Figure S4A, S4C, and S4D) (accumulated toxicity upon combined conditions of iron depletion/overload and Actinomycin D, however, prevented a fully rigorous assessment of half-lives across the time course of the experiment). We did observe, however, differential stability of the isoforms upon ACO1 knockdown (Figure S4B), indicating that RNA decay may contribute to the effects of some of the regulators identified in our screen.

To evaluate the functional consequences of iron-mediated regulation of Fas/CD95 splicing, anti-Fas antibodies were used to induce Fas-mediated apoptosis in peripheral blood mononuclear cells (PBMCs) exposed to Hemin or Desferal. The experiment was carried out in control cells or in cells induced

(D) GO enrichment analysis of molecular functions, calculated using GOrilla software. Enrichment p values are color coded as indicated at the bottom.
(E) Pie chart showing the functional classification of genome-wide screen hits. Class assignment was curated manually through available bibliography and information obtained from the DAVID GO database. Numbers represent the percentage of genes included in each of the categories. See also Figures S1 and S2 and Tables 1, 2, S2, and S3.

Table 1. Regulators of Fas/CD95

Splicing Components Involved in Fas AS Regulation		
Gene Symbol	(PSI) (Control Mean = 94.7)	p Value
SR proteins		
SFRS6	77.40	8.75×10^{-9}
SFRS1	99.11	1.60×10^{-2}
Non-snRNP spliceosome-assembly proteins		
SIAHBP1	63.27	2.00×10^{-5}
U2AF2	75.70	4.21×10^{-10}
U2AF1	65.11	7.74×10^{-14}
FNBP3	74.30	5.46×10^{-3}
U2 snRNP-specific proteins		
SF3B1	28.67	1.13×10^{-24}
SF3B2	54.27	4.41×10^{-18}
SF3B3	50.22	2.51×10^{-21}
SF3A1	55.32	7.25×10^{-20}
SF3A2	87.16	1.21×10^{-4}
SF3A3	50.66	4.63×10^{-20}
SF3B4	77.87	5.81×10^{-10}
SNRPA1	57.36	3.30×10^{-14}
U5 snRNP-specific proteins		
PRPF8	53.86	2.10×10^{-4}
U5-200KD	70.94	1.01×10^{-2}
U4/U6 snRNP-specific proteins		
PPIH	63.59	3.77×10^{-3}
Sm/LSm core proteins		
SNRPB	78.84	8.57×10^{-8}
SNRPD1	85.22	6.52×10^{-4}
SNRPD2	80.65	3.33×10^{-5}
SNRPD3	59.91	8.06×10^{-7}
SNRPF	71.87	9.49×10^{-4}
SNRPG	75.43	3.20×10^{-2}
Catalytic step II and late-acting proteins		
DHX8	76.77	2.72×10^{-2}
SLU7	71.32	1.19×10^{-3}
CDC40	78.09	1.61×10^{-10}
Exon Junction complex		
RNPS1	72.21	1.56×10^{-3}
RBM8A	63.43	6.06×10^{-4}
Other previously reported splicing factors/SAPs		
TCERG1	82.48	2.31×10^{-5}
IK	58.75	3.10×10^{-9}
RRM-containing proteins		
RNPC2	42.94	2.08×10^{-10}
DExD box proteins		
DDX48	77.55	3.71×10^{-2}
Proteins with other known motifs		
XAB2	53.59	4.75×10^{-19}
ZNF207	74.07	6.94×10^{-7}
Proteins designated as H complex components		
BUB3	86.52	3.09×10^{-5}
Others		
EWSR1	74.02	3.43×10^{-6}
SFPQ	73.87	3.81×10^{-7}
Group 1 (Early splicing factors)		
THRAP3	60.12	2.28×10^{-3}
Group 2 (B complex stage)		
SMU1	23.79	9.82×10^{-27}
AQR	71.81	7.39×10^{-9}
Group 3 (C complex stage)		
LENG1	65.70	7.80×10^{-4}

Spliceosome components whose knockdown in HeLa cells affects the ratio between inclusion and skipping of endogenous Fas/CD95 exon 6 are shown. Factors are classified according to functional categories and/or spliceosomal subcomplexes. PSI values correspond to data from the final validation round of the screen for regulators of Fas exon 6 AS. p values represent statistical significance of Welch's t test between siRNA treatments compared to mock transfected samples.

to proliferate by treatment with phyto-haemagglutinin (PHA), which is known to promote a switch toward higher levels of Fas/CD95 exon 6 inclusion and apoptosis, a situation that mimics the physiological switch that eliminates expanded populations of T lymphocytes upon antigen clearance (Liu et al., 1995). Failure to undergo this switch leads to ALPS (Roesler et al., 2005), a nontumor condition characterized by persistent high levels of T cells. The results of Figures 3G, S4G, and S4H recapitulate in human T lymphocytes the changes in Fas exon 6 splicing upon iron overload and depletion observed in cell lines. Consistent with the predicted effects of the splicing changes, iron depletion (which promotes the soluble Fas isoform) protects T lymphocytes from Fas-mediated apoptosis, while iron excess tends to enhance it (Figures 3H, S4E, and S4F). While it was technically difficult to evaluate Fas/CD95 protein isoform levels in these cells, the results suggest that the ss switches induced in Fas/CD95 by regulation of iron levels are biologically relevant (see also Discussion).

Functional Connections between the Spliceosome and Iron Metabolism

To further explore the mechanisms by which iron levels can influence AS, we took advantage of a functional splicing network developed in our laboratory (accompanying manuscript by Papasaikas et al., 2015). The network was built by evaluating the effects of knocking down each of the known protein components of the splicing machinery on 35 AS events important for cell proliferation and apoptosis and quantitatively comparing the similarities between the effects of knockdown for every pair of spliceosomal components. We compared the effects of Hemin and Desferal treatments as well as the effects of depletion of ACO1 and FTL on these 35 AS events to those of splicing factors knockdowns. The network captured antagonistic effects between Hemin and Desferal, as well as similarities between the effects of Hemin and FTL depletion (Figure 4A), indicating that

Table 2. Other Regulators of Fas AS

Other Regulators of Fas AS		
Gene Symbol	(PSI) (Control Mean = 94.7)	p Value
Chromatin remodeling and histone modification		
SMARCA4	93.17	2.73×10^{-2}
SMARCC2	91.02	1.47×10^{-1}
SMARCD1	97.09	2.66×10^{-1}
SAP18	85.85	1.82×10^{-3}
SETD2	69.50	1.84×10^{-4}
Transcription factors		
MYBL1	87.67	4.37×10^{-1}
MYC	69.86	3.66×10^{-4}
DSCR6	51.92	1.37×10^{-4}
SNW1	61.53	3.06×10^{-6}
ZNF207	74.07	6.94×10^{-7}
ZNF830	87.52	1.15×10^{-3}
Topoisomerase and RNA pol II complex		
TOP2A	89.03	4.24×10^{-2}
TOPBP1	79.50	4.62×10^{-6}
POLR2F	84.83	1.72×10^{-2}
HOX-related genes		
HOXA10	88.78	6.48×10^{-1}
HOXB2	83.92	3.05×10^{-2}
HOXD9	88.22	6.34×10^{-1}
PKNOX1	89.97	6.23×10^{-1}
DNA repair		
XRCC2	92.87	5.33×10^{-1}
XRCC5	92.83	3.94×10^{-2}
RNA transport/THOC complex		
CSE1L	86.81	1.01×10^{-1}
THOC5	93.33	6.32×10^{-1}
THOC6	83.33	2.26×10^{-7}
THOC7	85.85	4.45×10^{-3}
Signal transduction pathways		
FGFR1	60.70	2.14×10^{-7}
MC1R	81.96	2.90×10^{-2}
RAB7A	92.93	4.61×10^{-1}
RAC2	91.65	2.86×10^{-3}
RALA	87.93	4.88×10^{-4}
RHOG	90.69	1.47×10^{-2}
WNT4	90.44	2.26×10^{-3}
WNT6	92.80	5.51×10^{-1}
Cellular metabolism		
ACADSB	50.41	5.25×10^{-8}
PDP2	64.63	2.30×10^{-6}
ALAD	60.82	6.22×10^{-5}
ATP5B	67.15	1.43×10^{-3}
Iron-homeostasis-related genes		
ACO1	70.05	1.24×10^{-5}
FTL	96.08	2.21×10^{-1}
B2M	88.94	6.55×10^{-1}
PCBP2	76.27	1.55×10^{-4}

Table 2. *Continued*

Regulators of Fas/CD95 exon 6 AS in other processes and pathways are shown. PSI and statistical significance values as in Table 1.

iron levels regulate multiple AS events. A very significant correlation (0.67) was found between the effects of Hemin treatment and the knockdown of the splicing factor SRSF7 (a classical SR protein family member) (Figures 4A, 4B, and S5A), indicating that iron overload induces changes in AS that closely resemble those induced by a reduction in SRSF7 activity. In agreement with this, overexpression of SRSF7 led to increased levels of Fas/CD95 exon 6 skipping, the opposite effect of Hemin treatment (Figure 4C). The similarities between SRSF7 depletion and Hemin treatment were particularly noticeable for AS events in the genes H2AFγ, GADD45A, and the apoptosis regulator DIABLO (Figures 4B and S5). Indeed, reciprocal effects were observed for Hemin/SRSF7 knockdown and Desferal/Ciclopirox treatments on DIABLO exon 4 inclusion levels (Figure 4D), confirming that iron homeostasis has a variety of effects on AS regulation.

Iron Disrupts SRSF7 Binding In Vivo and In Vitro

To investigate how iron-mediated AS modulation connects to SFRS7, we first considered the possibility that iron overload could decrease SRSF7 levels in the cell or modify its intracellular distribution. No significant effects were observed upon Hemin treatment, however, in the levels of SRSF7 mRNA (Figure S6A), SRSF7 protein (Figure 5A), or SRSF7 subcellular distribution (Figures 5B and S6B).

Next, we considered whether iron levels could affect the activity of SRSF7. SRSF7 is a classical member of the SR protein family of splicing regulators and the only one containing a Zinc-knuckle motif, which is known to be important for SRSF7 binding specificity (Cavaloc et al., 1999). To address potential effects of iron on SRSF7 binding, crosslinking immunoprecipitation (CLIP) experiments were carried out with a tagged version of SRSF7 in control or Hemin-treated HeLa cells. After RNA isolation, the association of SRSF7 with different regions of Fas/CD95 alternatively spliced region was tested by qPCR using consecutive 80-nt amplicons covering the alternatively spliced genomic sequences of Fas/CD95 from exon 5 to exon 7. Two main peaks of SRSF7 binding were detected in intron 6 (Figure 5C). The peaks overlap with sequences predicted to contain high-affinity binding sites for SRSF7 (Paz et al., 2010; Ray et al., 2013) (Figure 5C). Of relevance, binding of SRSF7 to these peaks was decreased under conditions of iron overload (Figure 5C). To further analyze the extent and specificity of these effects, the CLIP signals of endogenous SRSF7—or SRSF1 as a control—in three predicted and/or observed SRSF7 binding sites in the Fas/CD95 alternatively spliced region were quantified by real-time qPCR. The results showed a consistent decrease in SRSF7 binding to these regions upon conditions of iron

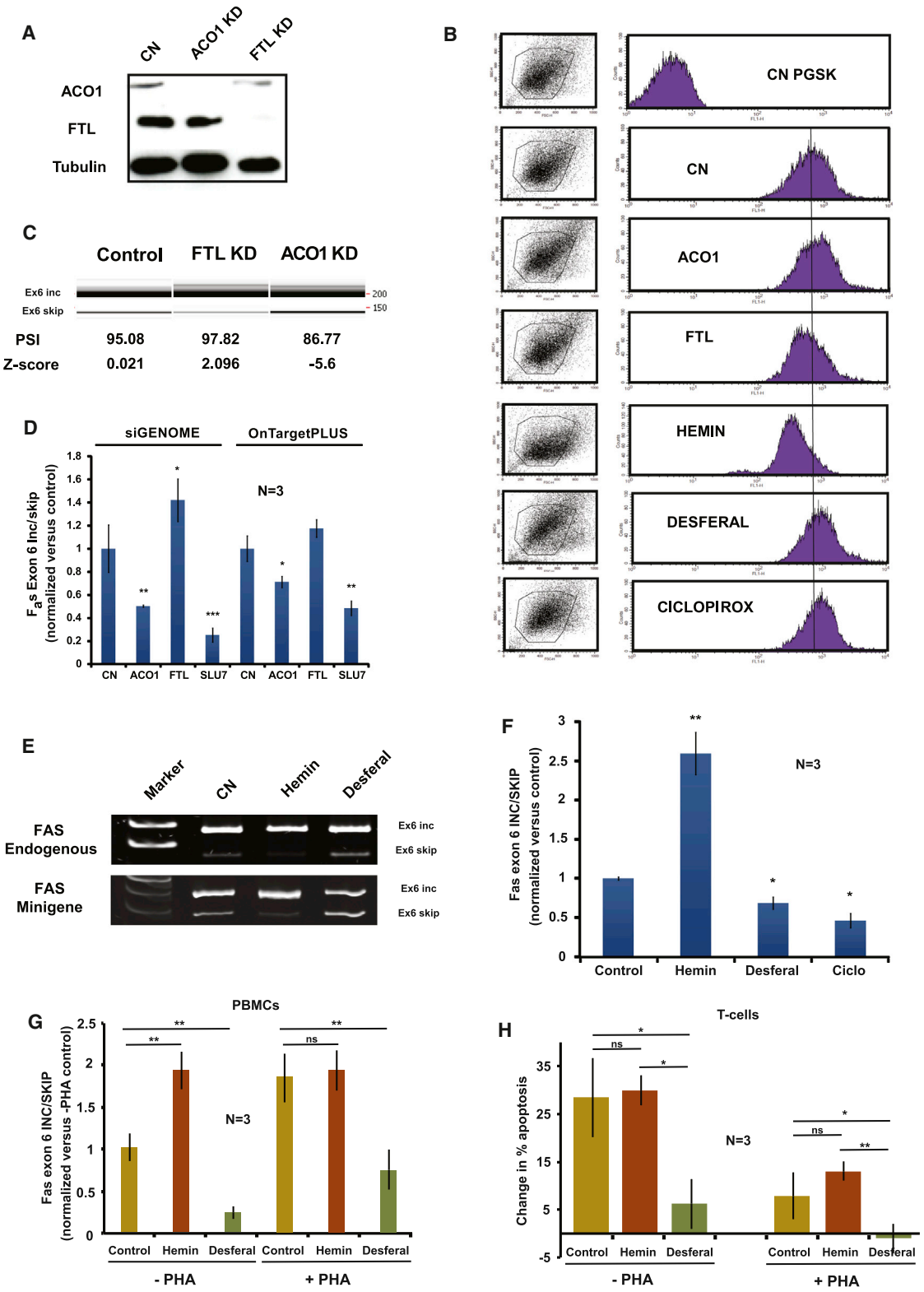

Figure 3. Iron Homeostasis Modulates Fas/CD95 AS

(A) Depletion of ACO1 and FTL protein levels by siRNA-mediated knockdown using SiGENOME library. Proteins were detected by western blot analysis under the indicated conditions. CN indicates mock siRNA-transfected cells.

(legend continued on next page)

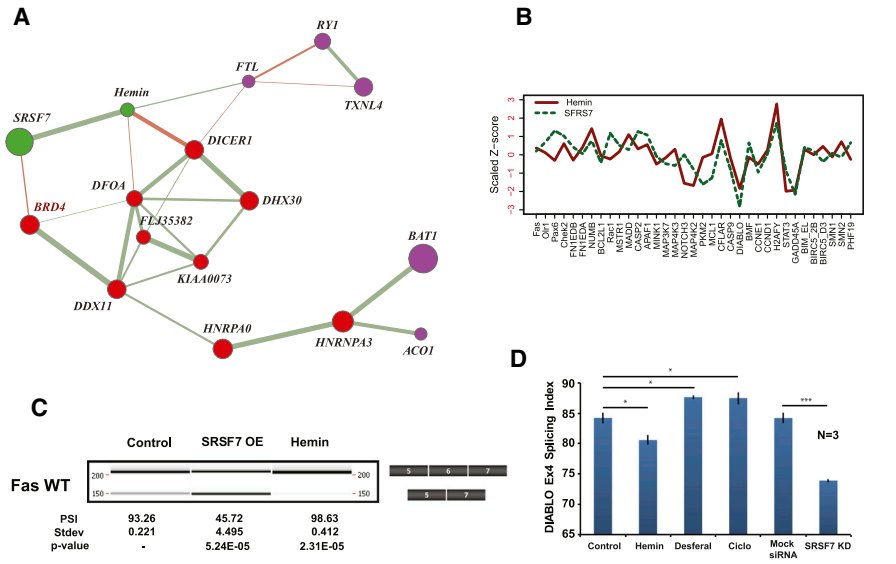

Figure 4. Functional Link between SRSF7 and Iron Homeostasis-Induced AS

(A) Functional links between RNA processing factors and alterations of iron levels, derived from a Splicing network analysis. Lines connecting RNA processing factors and treatments leading to changes in iron levels indicate similar (green) or opposite (red) effects on the profile of AS changes of 36 genes induced by splicing factor or ACO1/FTL knockdown or by treatment with 100 μM Hemin/Desferal (DFOA). Line widths are proportional to the strength of the correlations observed.

(B) Perturbation profile of AS changes upon SRSF7 knockdown or Hemin treatment across 36 AS events, analyzed by RT-PCR and capillary electrophoresis. Results correspond to scaled *Z* score changes from six biological replicas. Positive and negative *Z* scores indicate increased exon inclusion or skipping, respectively.

(C) SRSF7 overexpression and iron overload have antagonistic effects on Fas/CD95 AS. HeLa cells were transfected with a reporter minigene corresponding to Fas/CD95 exons 5–7 and either an empty vector or a SRSF7 expression vector and treated either with DMSO (control) or with 100 μM Hemin; RNAs were isolated and the patterns of Fas/CD95 AS analyzed by capillary electrophoresis. PSI indexes, SD, and p values for three independent experiments are shown.

(D) Effects of iron levels perturbation and SRSF7 knockdown on AS of the apoptosis regulatory gene DIABLO. Relative levels of DIABLO exon 4 inclusion were measured in RNAs from HeLa cells upon treatment with 100 μM Hemin, Desferal, or Cyclopirox or mock or SRSF7 knockdown by RT-PCR and capillary electrophoresis. Results correspond to the mean and SD of three biological replicates. p values obtained from Welch's t test are indicated: * 0.05 to 0.01; *** < 0.001. See also Figure S5.

overload, while SRSF1 (another SR protein lacking a Zn-knuckle; Figure 6A) binding was only marginally decreased or even increased (perhaps due to the loss of competitor SRSF7 binding) upon iron excess (Figures 5D–5F). Consistent with the concept that these binding events are relevant for SRSF7-mediated repression, deletion of a region containing the most prominent SRSF7 binding peak in intron 6 led to increased exon inclusion (Figures 5G–5I and S5C). In addition, deletion of this SRSF7 binding site reduced (but did not abolish) the effect of SRSF7 overexpression, suggesting that this and other SRSF7 binding sites contribute to regulation. SRSF7-mediated repression is significantly more compromised in the mutant under conditions of iron overload (Figure 5I), suggesting synergistic effects between the loss of SRSF7 binding sites and reduced SRSF7 binding affinity. Collectively, the results are consistent with a model where iron levels modulate the RNA binding properties of this Zinc-knuckle-containing protein, and this, in turn, regulates Fas/CD95 AS.

To test whether iron can have a direct effect on RNA recognition by SRSF7, recombinant SRSF7 protein expressed in and purified from *E. coli* was partially denatured and refolded in the presence of Fe^{2+} or Zn^{2+} and binding to previously described

(B) Analysis of intracellular iron levels by Phen-green SK fluorescence flow cytometry. HeLa cells transfected with siRNAs against ACO1 or FTL, or treated with 100 μM Hemin (to induce iron overload) or 100 μM Desferal or cyclopirox olamine (to induce iron depletion) were FACS-sorted (left panels) and the geometric median of Phen-green SK fluorescence intensity for a representative experiment is shown (right panels). The x axis represents fluorescence intensity, and the y axis represents cell numbers. CN PGSK indicates autofluorescence in the absence of Phen-green SK treatment. CN corresponds to control cells transfected with scrambled siRNAs and incubated with DMSO instead of of Hemin or Desferal. ACO1 and FTL knockdown treatments were also incubated with DMSO prior to experimental measurements.

(C) RT-PCR analysis of Fas/CD95 exon 6 AS upon FTL or ACO1 knockdown, analyzed by capillary electrophoresis. PSI index and *Z* score values are indicated.

(D) Real-time qPCR analysis of Fas/CD95 exon 6 AS upon FTL, ACO1, or SLU7 knockdown in HeLa cells using two independent siRNA libraries.

(E) RT-PCR analysis of Fas/CD95 AS upon treatment of HeLa cells with 100 μM Hemin (to induce iron overload) or 100 μM Desferal (to induce iron depletion). Both endogenous transcripts (upper panel) or transcripts derived from an expression vector containing Fas/CD95 genomic sequences from exons 5 to 7 (lower panel, analyzed using vector-specific primers) were analyzed.

(F) Real-time qPCR analysis of Fas/CD95 AS in HeLa cells treated with 100 μM Hemin, Desferal, or cyclopirox olamine.

(G) Real-time qPCR analysis of Fas/CD95 exon 6 AS in RNAs from human peripheral blood mononuclear cells (PBMCs) untreated or treated with PHA (2 μM) for 48 hr upon changes in iron levels induced by treatment with 100 μM Hemin, 100 μM Desferal, or DMSO for 12 hr. Values were normalized to the control minus PHA condition. For (C)–(G), values represent the mean and SD of three biological replicas. p values obtained from Welch's t test are indicated: * 0.05 to 0.01, ** 0.01 to 0.001, and *** < 0.001.

(H) Induction of Fas-mediated apoptosis in human PBMCs upon modulation of iron levels. Data represent the percentage of change in apoptotic cells upon treatment of human PBMCs with Fas antibody (1 μg) or isotype control IgG for 16 hr. Cells were previously exposed (or not) to PHA (2 μM) for 48 hr and to either 100 μM Hemin, 100 μM Desferal, or DMSO for 12 hr. Cells were FACS sorted with anti-CD3 antibodies to select T lymphocyte populations and apoptosis induction was normalized to control minus PHA condition. Values represent the mean and SD of three independent biological replicas, and p values from Welch's one-tailed t test are indicated: * 0.05 to 0.01, ** 0.01 to 0.001, and *** < 0.001. See also Figures S3 and S4.

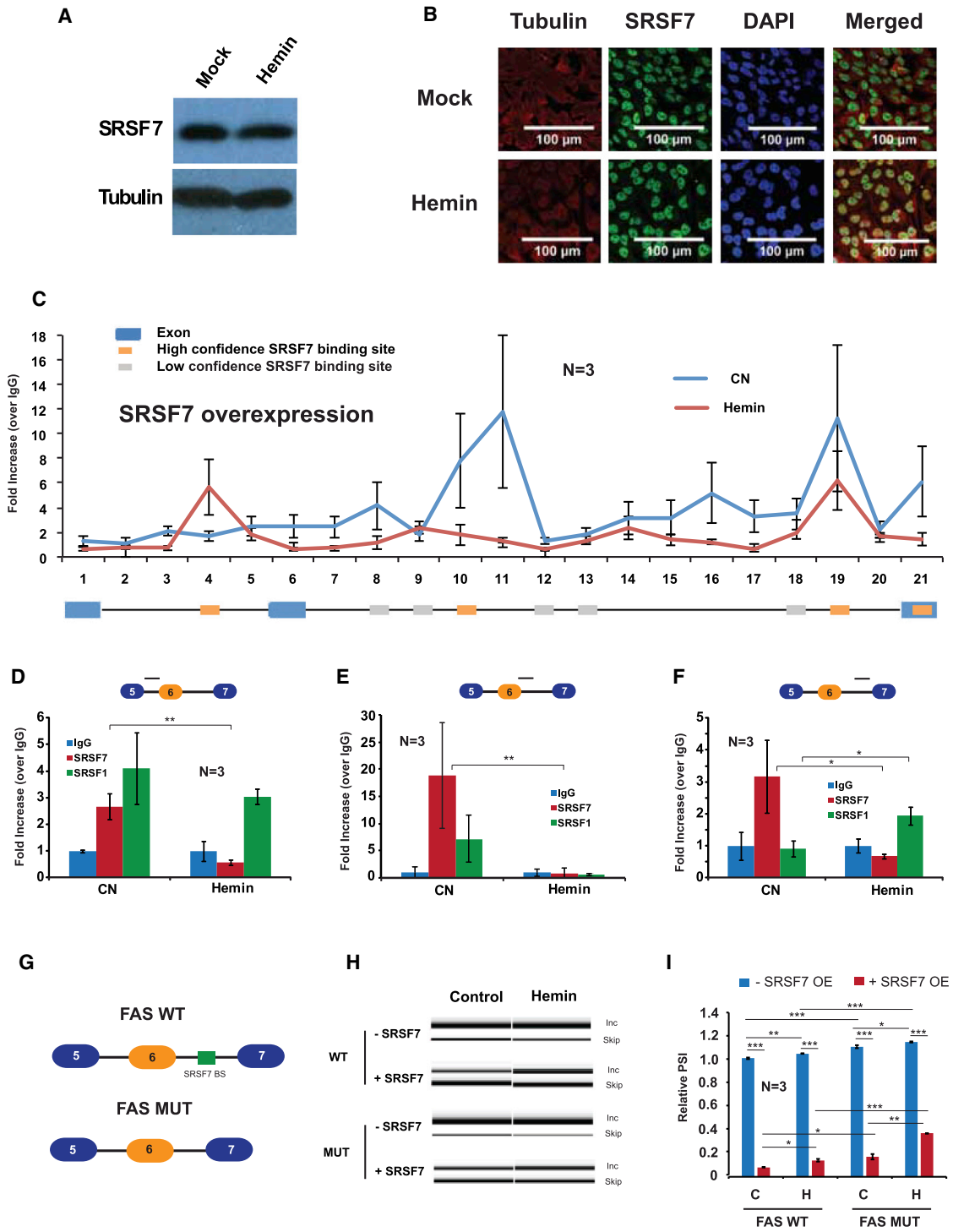

Figure 5. Iron Regulates SRSF7 RNA Binding

(A) SRSF7 protein levels are not significantly affected by increased iron. HeLa cells were treated with DMSO or 100 μM Hemin for 24 hr and the levels of SRSF7 protein analyzed by western blot.

(B) SRSF7 intracellular localization is not affected by increased iron. SRSF7 was detected in DMSO- or 100 μM Hemin-treated cells by immunofluorescence using specific antibodies. Tubulin and DAPI staining and tubulin/SRSF7 overlay staining are also shown.

(C) Identification of SRSF7 binding sites in Fas/CD95 AS region by in vivo CLIP. HeLa cells transfected with epitope-tagged SRSF7 were UV light irradiated and lysed, and RNA present in SRSF7 immunoprecipitates was analyzed by RT-PCR using amplicons covering Fas/CD45 genomic region from exon 5 to 7 in control

(legend continued on next page)

SRSF7 SELEX RNA motifs tested in filter binding assays. Refolding of SRSF7 in the presence of Zn^{2+} enhanced RNA binding, while refolding in the presence of Fe^{2+} decreased binding to this RNA (Figure 6C). These differences were negligible when a SRSF7 variant lacking the Zinc-knuckle domain (Figures 6A and 6D) or when the binding of another SR protein, SRSF1 (Figure 6E), were tested. The differences were also negligible when binding to another RNA motif recognized by SRSF7 RRM domain (Cavaloc et al., 1999) was tested (Figures 6F–6H), indicating that the differential effects of Zn^{2+} and Fe^{2+} depend on the RNA binding activity of the Zinc-knuckle domain. No significant decrease in RNA interactions induced by Fe^{2+} was observed when binding of U2AF65 RRMs 1 + 2 to a pyrimidine-rich target site was tested (Figure 6B), again arguing that the effects of Fe^{2+} on RNA binding are specific of Zn-knuckle-containing motifs.

We conclude that iron levels can modulate the RNA binding activity of SRSF7 through its Zn-knuckle domain and that this impinges on SFRS7-mediated AS regulation (Figure 6I).

DISCUSSION

Our automatized screening strategy allows the rapid identification of AS regulators of endogenous transcripts in human cells. It offers a number of advantages over reporter-based screenings, including the direct analysis of transcript isoforms (in contrast to readouts that require accumulation of protein products, which can be affected by effects on mRNA translation and stability of fluorescent proteins or enzymatic activities). The transcripts are generated in physiological amounts at endogenous chromatin loci, rather than from partial genomic regions engineered into expression vectors driven by different promoters/3′ end formation signals and either episomically expressed or integrated in different copy numbers and genomic loci. Our method can be applied to any siRNA-transfectable cell line and generates, as an initial product of the screen, a library of tens of thousands transcriptomes that, combined with PCR barcoding and deep sequencing, allows sensitive and accurate analyses of the regulation of transcription, splicing, polyadenylation, or RNA decay for any human gene expressing coding or long noncoding RNAs.

In this study we identified 200 genes whose knockdown causes changes in Fas/CD95 AS. Given the stringent filters applied, SRSF7 was not identified as a regulator in the initial screen, suggesting that our method is likely to miss a fraction of bona fide splicing regulators. Nevertheless, our unbiased search rendered known and classical regulators of AS, including SR proteins like SRSF1 and SRSF6 (Cléry et al., 2013). The bulk of the splicing factors identified as regulators, however, correspond to core components of the splicing machinery. Remarkably, these include factors involved at essentially every stage of spliceosome assembly, indicating that regulation of AS can be achieved not only at early stages of ss recognition but also throughout the complex spliceosomal cycle, even for factors that function in the process of catalytic activation of the spliceosome. This implies extensive functional flexibility and potential for reversibility in the assembly of these complexes (Hoskins and Moore, 2012). While several previous reports provided evidence that particular components of the core splicing machinery can influence AS (Clark et al., 2002; Park et al., 2004; Pleiss et al., 2007; Saltzman et al., 2011) the results of our unbiased screen reveal the extensive remarkable potential of the core splicing machinery to regulate ss choice (see also accompanying manuscript by Papasaikas et al., 2015).

Links between Fas/CD95 AS and Other Cellular Processes

Consistent with the results of a recent systematic reverse genetic screen for factors that impact pre-mRNA splicing in budding yeast (Albulescu et al., 2012), we identified multiple factors involved in transcription and chromatin remodeling as regulators of Fas/CD95 AS. Some of these effects may be indirectly mediated by changes in the expression of classical splicing regulators. Thus, the transcription factor Myc—which we found to influence Fas/CD95 AS—is known to regulate transcription of several hnRNP proteins like hnRNP A1/B2 and PTB (David et al., 2010), the latter known to promote Fas exon 6 skipping through an exonic silencer sequence (Izquierdo et al., 2005). Direct effects of transcription/chromatin structure on Fas/CD95 AS are also likely. Results from numerous studies are consistent with the idea that kinetic competition between ss can be modulated by changes in transcription elongation rates (de la Mata et al., 2003; Ip et al., 2011; Soret et al., 2003; Solier et al., 2004; Solier et al., 2010; reviewed by Dujardin et al., 2013). Our identification of a subunit of RNA polymerase II, topoisomerase 2 alpha, and topoisomerase 2-binding protein 1 as regulators of Fas/CD95 AS may be explained by the function of these proteins in transcription elongation. Furthermore, nucleosome density and epigenetic marks have been linked to efficient ss recognition/regulation through effects on transcription elongation or cotranscriptional recruitment of splicing factors (Batsché et al., 2006; Chen et al., 2009; de Almeida et al., 2011; Moehle

(CN) cells or cells treated with 100 μM Hemin for 24 hr. Binding values represent mean and SD of fold-increase over control IgG for three independent experiments, after normalization by input levels of each amplicon and condition. The positions of exons and predicted SRSF7 binding sites are indicated.

(D–F) Quantification of CLIP signals using antibodies against endogenous SRSF7 or SRSF1 in control or iron overload conditions (Hemin 100 μM for 24 hr), normalized to IgG background signals, for the three (high-confidence) predicted SRSF7 binding sites indicated. Values represent mean and SD for three independent biological replicates. The apparent discrepancy between the effects of Hemin treatment on the binding of SRSF7 in (C) and (D) may be due to overexpression of SRSF7 in the experiments of (C).

(G) Schematic diagram of the deletion mutant lacking the region containing the peak of SRSF7 binding in intron 6.

(H) Effects of SRSF7 overexpression on Fas exon 6 splicing using wild-type or mutant minigenes under control conditions or conditions of iron overload (Hemin), analyzed as in Figure 4C.

(I) Quantification of relative PSI values upon SRSF7 overexpression under control or iron overload conditions. Values represent mean and SD for three biological replicas. p values obtained from Welch's t test are indicated: * 0.05 to 0.01, ** 0.01 to 0.001, and *** < 0.001. See also Figure S6.

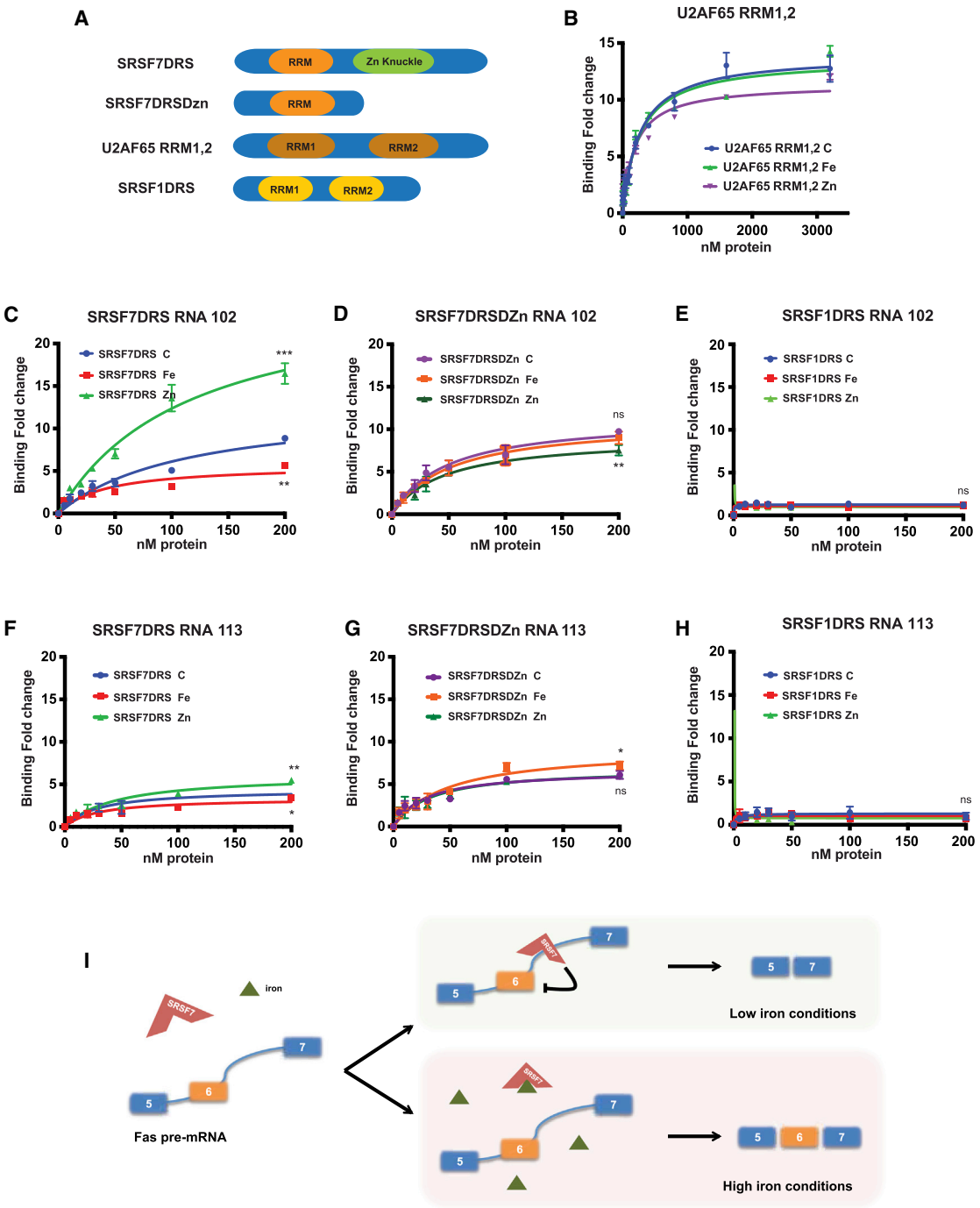

Figure 6. SRSF7 RNA Binding Properties Are Affected by Iron Abundance

(A) Domain representation of the proteins used for RNA binding assays (Mackereth et al., 2011; Cavaloc et al., 1999). RRM indicates RNA recognition motif. DRS and DZn indicate constructs lacking the RS motif or the Zinc finger, respectively.

(B) Filter binding assays representing fold enrichment of GST-U2AF65 RRM1&2 binding to UUUUUUUUUUUUUAG RNA after protein refolding in the presence of 50 μM Fe^{2+}, Zn^{2+}, or control. Values represent mean and SD values for at least three independent experiments.

(C–H) Filter binding assays (as in [B]) for the indicated proteins (as in [A]) and RNAs after protein refolding in the presence of 50 μM Fe^{2+}, Zn^{2+}, or control. RNA 102 corresponds to the sequence GACAACGACGACGACUAGAA, previously characterized as a high-affinity site for SRSF7 Zinc-knuckle domain, and RNA 113 corresponds to the sequence ACAAUCAUCACAACAUCGACU, previously characterized as a high-affinity site for SRSF7 RRM domain (Cavaloc et al., 1999). p values obtained from Welch's t test are indicated: * 0.05 to 0.01, ** 0.01 to 0.001, and *** < 0.001.

(I) Working model of iron-mediated Fas AS regulation. SRSF7 binding to Fas pre-mRNA under low-iron conditions promotes exon 6 skipping, while iron overload compromises the Zn-knuckle-domain-mediated RNA binding of SRSF7, leading to higher levels of exon 6 inclusion.

et al., 2012; Albulescu et al., 2012; reviewed by Luco et al., 2011). This may be also at the basis of the effects of knockdown of various components of the SWI/SNF chromatin remodeling complex and of the H3K36 methyl-transferase SETD2 on Fas/CD95 AS. The latter observation may be related to recent reports that the splicing process promotes the association of SETD2 with exonic genomic regions, with the consequent enrichment in the H3K36me3 mark (de Almeida et al., 2011; Kim et al., 2011), which appears to be differentially enriched in constitutive and alternative exons (Huff et al., 2010).

Links were also established with intracellular signaling pathways, including FGFR1. FGFR1 knockdown led to an increase in Fas/CD95 exon 6 skipping, an observation that can provide new mechanistic insights on the well-established function of this receptor on apoptosis control, influencing cell proliferation and differentiation (Acevedo et al., 2009). Three nuclear-encoded mitochondrial proteins were found to influence Fas/CD95 exon 6 inclusion: an acyl CoA-dehydrogenase involved in the first step in fatty acid β-oxidation, a catalytic subunit of pyruvate dehydrogenase phosphatase involved in the control of the primary link between glycolysis and the TCA cycle, and the β subunit of ATP synthetase. All three factors promote energy consumption and ATP generation, and mutations in some of them are associated with metabolic diseases, including intolerance to hypoglycemia or insulin resistance. While understanding the biological relevance of these links requires further investigation, an interesting possibility is that the cell's metabolic (e.g., oxidative phosphorylation) status relays signals that influence AS to trigger responses relevant to cell fate, proliferation, or programmed cell death. Indeed, AS of the pyruvate kinase (PKM) gene regulates the switch between aerobic and anaerobic glycolysis, which is relevant during development and for the proliferation of cancer cells (Christofk et al., 2008). It is therefore conceivable that the cell's metabolic status, in turn, regulates AS as part of feedback mechanisms of energy homeostasis.

Iron Homeostasis and AS Modulation

The opposite effects of knockdown of ACO1 and FTL genes—which have antagonistic roles in iron homeostasis—on Fas/CD95 AS led us to investigate in detail possible links between iron levels and Fas/CD95 exon 6 splicing. ACO1 is the enzyme that coverts citrate in isocitrate in the TCA cycle, an activity for which an iron-sulfur cluster plays an essential role. In the absence of iron, ACO1 is an RNA binding protein that binds sequence motifs known as iron-responsive elements (IREs), present in 5′ or 3′ UTRs of mRNAs to regulate the translation or decay of transcripts encoding proteins important for iron mobilization or storage (reviewed by Campillos et al., 2010; Sanchez et al., 2011). We first considered the possibility that ACO1 directly regulates Fas/CD95 AS or indirectly through the control of the levels of a splicing regulator. However, no IREs were predicted in the AS region, and the levels of SRSF7, identified as a regulator of Fas/CD95 AS through our functional network analysis, did not vary upon iron overload. Interestingly, we observed a significant correlation between the effects of intracellular iron levels and the presence of ACO1, suggesting that iron abundance, rather than ACO1 binding, is responsible for the effects observed in Fas/CD95 AS regulation, uncoupling the direct versus indirect effects of ACO1 in the iron homeostasis response (Figure S7).

The functional splicing network analysis also identified functional links between DICER1, the RNase III enzyme involved in processing of miRNA precursors, and different conditions of iron level manipulation. A recent report by Li et al. (2012) described a role for iron homeostasis in the modulation of DICER1 processivity, mediated by differential interaction with the iron sensor protein PCBP2. Interestingly, PCBP2 was also identified in our screen as a factor whose knockdown promotes Fas/CD95 exon 6 skipping (Table 2). It is conceivable that DICER1/PCBP2 knockdown leads to altered miRNA profiles and consequently to misregulation of splicing factors important for Fas exon 6 inclusion.

The activity of SR proteins as splicing regulators is often modulated in response to external stimuli through a variety of mechanisms, including posttranslational modifications and changes in subcellular localization (Blaustein et al., 2005; Zhou et al., 2012). SRSF7 is a nucleocytoplasmic shuttling SR protein involved in splicing regulation and mRNA export (Huang and Steitz, 2001; Huang et al., 2004), and changes in protein localization upon different stress stimuli have been proposed as a potential mechanism for modulation of SRSF7 activity in plants (Rausin et al., 2010). Our experiments did not reveal substantial changes in SRSF7 protein levels or localization upon variations in iron levels, but rather a direct effect of iron in the RNA binding properties of the Zn-knuckle domain of SRSF7, which has been shown to confer differential RNA binding specificities to this SR protein (Cavaloc et al., 1999).

Zn fingers usually require Zinc ions to maintain their folding and nucleic acid binding activities, although studies involving tristetraproline protein reported that substitution of zinc by iron does not compromise the RNA binding activities of the protein (Conte et al., 1996; diTargiani et al., 2006). This is in contrast with SRSF7, where in vivo and in vitro results are consistent with decreased RNA binding activity of the Zinc-knuckle in the presence of iron, leading to effects on Fas/CD95 AS that are similar to those induced by SRSF7 knockdown. A parallel can therefore be made between ACO1 and SRSF7, because high levels of iron reduce the activities of both proteins in RNA binding and post-transcriptional gene regulation. Similar effects on other Zinc-dependent nucleic acid binding factors may induce changes in AS or in other steps of transcriptional or posttranscriptional regulation that help to respond to changes in iron levels.

While the physiological context in which Fas/CD995 splicing plays a role in the response to changes in iron levels requires further studies, our results suggest that iron-mediated modulation of Fas/CD95 AS has consequences for Fas-mediated apoptosis of T lymphocytes, a physiologically important process that serves to eliminate expanded populations of T cells after antigen clearance, alterations of which lead to the autoimmune disorder ALPS (Liu et al., 1995; Roesler et al., 2005). It is conceivable that perturbations in iron homeostasis affecting Fas/CD95 splicing and signaling will lead to alterations in T lymphocyte populations, and these, in turn, affect the function of the immune system. Indeed, associations have been found between high-level iron overload in Hereditary Hemochromatosis and reduced

levels/ alterations of particular populations of T lymphocytes (reviewed by Porto and De Sousa, 2007). Abnormally high iron uptake is also believed to contribute to necrosis and apoptosis of liver cells and to the development of hepatic fibrosis and cirrhosis (reviewed by Ramm and Ruddell, 2010). In addition to the well-known effects of elevated iron levels on the induction of oxidative stress, promoting the synthesis of the proapoptotic Fas isoform could contribute to trigger hepatocyte cell death.

In conclusion, our screening platform provides a valuable tool for the discovery of splicing regulators and of functional connections between AS and other cellular pathways. We uncovered a link between iron homeostasis and Fas/CD95 AS as well as a regulatory mechanism based on the effects of iron on the RNA binding properties of a Zinc-knuckle-containing splicing factor.

EXPERIMENTAL PROCEDURES

siRNA Transfection and High Throughput mRNA Isolation

HeLa cells were forward transfected in triplicate in 96-well plates with a siRNA library against known and predicted protein-coding human genes, comprising >21,000 siRNAs (genome-wide screen, SMARTpools siGENOME, Thermo-Scientific) or 250 spliceosome-related siRNAs (Pilot screen, SMARTpools ON TARGET PLUS, Thermo-Scientific) using an automatized robotic procedure (Sciclone Liquid Handling Workstation, Perkin Elmer). Cellular mRNAs were isolated 72 hr posttransfection by an automated procedure using oligo-dT-coated 96-well plates (mRNA catcher PLUS, Life Technologies) following the manufacturer's recommendations.

Reverse Transcription and Barcoded PCR

Isolated mRNAs were reverse transcribed in 96-cell plates with superscript III (Life Technologies) in the presence of oligo-dT (Sigma-Aldrich) and random primers (Life Technologies) following the manufacturer's instructions. Semi-quantitative barcoded PCR primer sets (280 forward, 96 reverse, Sigma-Aldrich, using barcode sequences previously reported by Hamady et al., 2008) were designed to amplify both Fas isoforms corresponding to the inclusion and skipping of Fas exon 6 (see Table S4). PCR reactions were performed with a specific combination of forward and reverse barcoded primers (See Table S2) and reagents provided in the GoTaq DNA polymerase kit (GoTaq, Promega). RT and PCR protocols were set up for 96-well plates and performed in a Zephyr compact liquid handling workstation (Perkin Elmer).

Multiplexed Assessment of AS by Deep Sequencing

For the analysis of the genome-wide screen, 26,880 PCR samples corresponding to the products of inclusion and skipping of Fas/CD95 exon 6 in different knockdown conditions were pooled and sequenced by Solexa paired-end deep sequencing at the EMBL genomic core facility. Paired-end sequencing allowed to determine, for each DNA molecule, the knockdown condition and the Fas/CD95 PSI value. Further details and alignment metrics are provided in Supplemental Experimental Procedures.

Hit Validation

Positive hits obtained in the deep sequencing analysis were selected and re-tested in biological triplicate by HTCE (Labchip GX, Perkin Elmer). To control for possible off-target effects, the 427 positive hits from the previous analysis were selected, and a custom independent siRNA library against those factors (On target PLUS smartpool, Thermo-Scientific) was used to transfect HeLa cells. RNAs were isolated and processed in triplicate as described above, and RT-PCR products for each condition were analyzed by HTCE.

CLIP

Ultraviolet-light-induced CLIP experiments were carried out essentially as described (Konig et al., 2011) using antibodies against the indicated proteins (further details in Supplemental Experimental Procedures). After the immunoprecipitation step, samples were treated with proteinase K, RNA was extracted by phenol-chloroform extraction followed by ethanol precipitation, and samples were reverse transcribed and analyzed by real-time qPCR.

Further detailed description of this and other experimental procedures can be found in Supplemental Experimental Procedures.

ACCESSION NUMBERS

Deep sequencing data corresponding to quantification of *Fas/CD95* isoforms under different knock down conditions have been deposited in the NCBI SRA database (SRA study accession SRP050031).

SUPPLEMENTAL INFORMATION

Supplemental Information includes seven figures, four tables, and Supplemental Experimental Procedures and can be found with this article online at http://dx.doi.org/10.1016/j.molcel.2014.10.029.

ACKNOWLEDGMENTS

We thank many CRG colleagues and EURASNET members for their advice, encouragement, and critical reading of the manuscript; M. López Montañés and M. López-Botet for their help to purify PBMCs; and J. Stévenin for reagents. We acknowledge the excellent technical support of the CRG Robotics, Cell Sorting, Genomics and Bioinformatic Facilities, and the EMBL Genomics facility. J.R.T. was supported by a PhD fellowship from Fondo de Investigaciones Sanitarias. Work in our lab is supported by Fundación Botín, Consolider RNAREG, Ministerio de Economía e Innovación, and AGAUR.

Received: March 25, 2014
Revised: September 24, 2014
Accepted: October 31, 2014
Published: December 4, 2014

REFERENCES

Acevedo, V.D., Ittmann, M., and Spencer, D.M. (2009). Paths of FGFR-driven tumorigenesis. Cell Cycle *8*, 580–588.

Albulescu, L.O., Sabet, N., Gudipati, M., Stepankiw, N., Bergman, Z.J., Huffaker, T.C., and Pleiss, J.A. (2012). A quantitative, high-throughput reverse genetic screen reveals novel connections between Pre-mRNA splicing and 5′ and 3′ end transcript determinants. PLoS Genet. *8*, e1002530.

Barbosa-Morais, N.L., Irimia, M., Pan, Q., Xiong, H.Y., Gueroussov, S., Lee, L.J., Slobodeniuc, V., Kutter, C., Watt, S., Colak, R., et al. (2012). The evolutionary landscape of alternative splicing in vertebrate species. Science *338*, 1587–1593.

Batsché, E., Yaniv, M., and Muchardt, C. (2006). The human SWI/SNF subunit Brm is a regulator of alternative splicing. Nat. Struct. Mol. Biol. *13*, 22–29.

Blaustein, M., Pelisch, F., Tanos, T., Muñoz, M.J., Wengier, D., Quadrana, L., Sanford, J.R., Muschietti, J.P., Kornblihtt, A.R., Cáceres, J.F., et al. (2005). Concerted regulation of nuclear and cytoplasmic activities of SR proteins by AKT. Nat. Struct. Mol. Biol. *12*, 1037–1044.

Braunschweig, U., Gueroussov, S., Plocik, A.M., Graveley, B.R., and Blencowe, B.J. (2013). Dynamic integration of splicing within gene regulatory pathways. Cell *152*, 1252–1269.

Campillos, M., Cases, I., Hentze, M.W., and Sanchez, M. (2010). SIREs: searching for iron-responsive elements. Nucleic Acids Res. *38*, W360–W367.

Cascino, I., Fiucci, G., Papoff, G., and Ruberti, G. (1995). Three functional soluble forms of the human apoptosis-inducing Fas molecule are produced by alternative splicing. J. Immunol. *15*, 2706–2713.

Cavaloc, Y., Bourgeois, C.F., Kister, L., and Stévenin, J. (1999). The splicing factors 9G8 and SRp20 transactivate splicing through different and specific enhancers. RNA *5*, 468–483.

Chen, L., Xiao, S., and Manley, N.R. (2009). Foxn1 is required to maintain the postnatal thymic microenvironment in a dosage-sensitive manner. Blood *113*, 567–574.

Chen, L., Park, S.M., Tumanov, A.V., Hau, A., Sawada, K., Feig, C., Turner, J.R., Fu, Y.X., Romero, I.L., Lengyel, E., and Peter, M.E. (2010). CD95 promotes tumour growth. Nature *465*, 492–496.

Cheng, J., Zhou, T., Liu, C., Shapiro, J.P., Brauer, M.J., Kiefer, M.C., Barr, P.J., and Mountz, J.D. (1994). Protection from Fas-mediated apoptosis by a soluble form of the Fas molecule. Science *263*, 1759–1762.

Chew, S.K., Chen, P., Link, N., Galindo, K.A., Pogue, K., and Abrams, J.M. (2009). Genome-wide silencing in Drosophila captures conserved apoptotic effectors. Nature *460*, 123–127.

Christofk, H.R., Vander Heiden, M.G., Harris, M.H., Ramanathan, A., Gerszten, R.E., Wei, R., Fleming, M.D., Schreiber, S.L., and Cantley, L.C. (2008). The M2 splice isoform of pyruvate kinase is important for cancer metabolism and tumour growth. Nature *452*, 230–233.

Clark, T.A., Sugnet, C.W., and Ares, M., Jr. (2002). Genomewide analysis of mRNA processing in yeast using splicing-specific microarrays. Science *296*, 907–910.

Cléry, A., Sinha, R., Anczuków, O., Corrionero, A., Moursy, A., Daubner, G.M., Valcárcel, J., Krainer, A.R., and Allain, F.H. (2013). Isolated pseudo-RNA-recognition motifs of SR proteins can regulate splicing using a noncanonical mode of RNA recognition. Proc. Natl. Acad. Sci. USA *110*, E2802–E2811.

Conte, D., Narindrasorasak, S., and Sarkar, B. (1996). In vivo and in vitro iron-replaced zinc finger generates free radicals and causes DNA damage. J. Biol. Chem. *271*, 5125–5130.

David, C.J., Chen, M., Assanah, M., Canoll, P., and Manley, J.L. (2010). HnRNP proteins controlled by c-Myc deregulate pyruvate kinase mRNA splicing in cancer. Nature *463*, 364–368.

de Almeida, S.F., Grosso, A.R., Koch, F., Fenouil, R., Carvalho, S., Andrade, J., Levezinho, H., Gut, M., Eick, D., Gut, I., et al. (2011). Splicing enhances recruitment of methyltransferase HYPB/Setd2 and methylation of histone H3 Lys36. Nat. Struct. Mol. Biol. *18*, 977–983.

de la Mata, M., Alonso, C.R., Kadener, S., Fededa, J.P., Blaustein, M.A., Pelisch, F., Cramer, P., Bentley, D., and Kornblihtt, A.R. (2003). A slow RNA polymerase II affects alternative splicing in vivo. Mol. Cell *12*, 525–532.

diTargiani, R.C., Lee, S.J., Wassink, S., and Michel, S.L. (2006). Functional characterization of iron-substituted tristetraprolin-2D (TTP-2D, NUP475-2D): RNA binding affinity and selectivity. Biochemistry *45*, 13641–13649.

Dujardin, G., Lafaille, C., Petrillo, E., Buggiano, V., Gómez Acuña, L.I., Fiszbein, A., Godoy Herz, M.A., Nieto Moreno, N., Muñoz, M.J., Alló, M., et al. (2013). Transcriptional elongation and alternative splicing. Biochim. Biophys. Acta *1829*, 134–140.

Fica, S.M., Tuttle, N., Novak, T., Li, N.S., Lu, J., Koodathingal, P., Dai, Q., Staley, J.P., and Piccirilli, J.A. (2013). RNA catalyses nuclear pre-mRNA splicing. Nature *503*, 229–234.

Fu, X.D., and Ares, M., Jr. (2014). Context-dependent control of alternative splicing by RNA-binding proteins. Nat. Rev. Genet. *15*, 689–701.

Gazin, C., Wajapeyee, N., Gobeil, S., Virbasius, C.M., and Green, M.R. (2007). An elaborate pathway required for Ras-mediated epigenetic silencing. Nature *449*, 1073–1077.

Gray, N.K., and Hentze, M.W. (1994). Iron regulatory protein prevents binding of the 43S translation pre-initiation complex to ferritin and eALAS mRNAs. EMBO J. *13*, 3882–3891.

Hamady, M., Walker, J.J., Harris, J.K., Gold, N.J., and Knight, R. (2008). Error-correcting barcoded primers for pyrosequencing hundreds of samples in multiplex. Nat. Methods *5*, 235–237.

Hentze, M.W., Muckenthaler, M.U., Galy, B., and Camaschella, C. (2010). Two to tango: regulation of Mammalian iron metabolism. Cell *142*, 24–38.

Hoskins, A.A., and Moore, M.J. (2012). The spliceosome: a flexible, reversible macromolecular machine. Trends Biochem. Sci. *37*, 179–188.

Huang, Y., and Steitz, J.A. (2001). Splicing factors SRp20 and 9G8 promote the nucleocytoplasmic export of mRNA. Mol. Cell *7*, 899–905.

Huang, Y., Yario, T.A., and Steitz, J.A. (2004). A molecular link between SR protein dephosphorylation and mRNA export. Proc. Natl. Acad. Sci. USA *101*, 9666–9670.

Huff, J.T., Plocik, A.M., Guthrie, C., and Yamamoto, K.R. (2010). Reciprocal intronic and exonic histone modification regions in humans. Nat. Struct. Mol. Biol. *17*, 1495–1499.

Ip, J.Y., Schmidt, D., Pan, Q., Ramani, A.K., Fraser, A.G., Odom, D.T., and Blencowe, B.J. (2011). Global impact of RNA polymerase II elongation inhibition on alternative splicing regulation. Genome Res. *21*, 390–401.

Izquierdo, J.M., Majós, N., Bonnal, S., Martínez, C., Castelo, R., Guigó, R., Bilbao, D., and Valcárcel, J. (2005). Regulation of Fas alternative splicing by antagonistic effects of TIA-1 and PTB on exon definition. Mol. Cell *19*, 475–484.

Katz, Y., Wang, E.T., Airoldi, E.M., and Burge, C.B. (2010). Analysis and design of RNA sequencing experiments for identifying isoform regulation. Nat. Methods *7*, 1009–1015.

Kim, S., Kim, H., Fong, N., Erickson, B., and Bentley, D.L. (2011). Pre-mRNA splicing is a determinant of histone H3K36 methylation. Proc. Natl. Acad. Sci. USA *108*, 13564–13569.

Konig, J., Zarnack, K., Rot, G., Curk, T., Kayikci, M., Zupan, B., Turner, D.J., Luscombe, N.M., and Ule, J. (2011). iCLIP–transcriptome-wide mapping of protein-RNA interactions with individual nucleotide resolution. J. Vis. Exp. *30*, http://dx.doi.org/10.3791/2638.

Kornblihtt, A.R., Schor, I.E., Alló, M., Dujardin, G., Petrillo, E., and Muñoz, M.J. (2013). Alternative splicing: a pivotal step between eukaryotic transcription and translation. Nat. Rev. Mol. Cell Biol. *14*, 6072–6083.

Krammer, P.H. (2000). CD95's deadly mission in the immune system. Nature *407*, 789–795.

Li, Y., Lin, L., Li, Z., Ye, X., Xiong, K., Aryal, B., Xu, Z., Paroo, Z., Liu, Q., He, C., and Jin, P. (2012). Iron homeostasis regulates the activity of the microRNA pathway through poly(C)-binding protein 2. Cell Metab. *15*, 895–904.

Liu, C., Cheng, J., and Mountz, J.D. (1995). Differential expression of human Fas mRNA species upon peripheral blood mononuclear cell activation. Biochem. J. *310*, 957–963.

Luco, R.F., Allo, M., Schor, I.E., Kornblihtt, A.R., and Misteli, T. (2011). Epigenetics in alternative pre-mRNA splicing. Cell *144*, 16–26.

Mackereth, C.D., Madl, T., Bonnal, S., Simon, B., Zanier, K., Gasch, A., Rybin, V., Valcárcel, J., and Sattler, M. (2011). Multi-domain conformational selection underlies pre-mRNA splicing regulation by U2AF. Nature *475*, 408–411.

Merkin, J., Russell, C., Chen, P., and Burge, C.B. (2012). Evolutionary dynamics of gene and isoform regulation in Mammalian tissues. Science *338*, 1593–1599.

Moehle, E.A., Ryan, C.J., Krogan, N.J., Kress, T.L., and Guthrie, C. (2012). The yeast SR-like protein Npl3 links chromatin modification to mRNA processing. PLoS Genet. *8*, e1003101.

Moore, M.J., Wang, Q., Kennedy, C.J., and Silver, P.A. (2010). An alternative splicing network links cell-cycle control to apoptosis. Cell *142*, 625–636.

Muckenthaler, M., Richter, A., Gunkel, N., Riedel, D., Polycarpou-Schwarz, M., Hentze, S., Falkenhahn, M., Stremmel, W., Ansorge, W., and Hentze, M.W. (2003). Relationships and distinctions in iron-regulatory networks responding to interrelated signals. Blood *101*, 3690–3698.

Neumann, B., Walter, T., Hériché, J.K., Bulkescher, J., Erfle, H., Conrad, C., Rogers, P., Poser, I., Held, M., Liebel, U., et al. (2010). Phenotypic profiling of the human genome by time-lapse microscopy reveals cell division genes. Nature *464*, 721–727.

Nilsen, T.W., and Graveley, B.R. (2010). Expansion of the eukaryotic proteome by alternative splicing. Nature *463*, 457–463.

Papasaikas, P., Ramón Tejedor, J., Vigevani, L., and Valcárcel, J. (2015). Functional splicing network reveals extensive regulatory potential of the core spliceosomal machinery. Mol. Cell *57*, this issue, 7–22.

Papoff, G., Cascino, I., Eramo, A., Starace, G., Lynch, D.H., and Ruberti, G. (1996). An N-terminal domain shared by Fas/Apo-1 (CD95) soluble variants prevents cell death in vitro. J. Immunol. *156*, 4622–4630.

Park, J.W., Parisky, K., Celotto, A.M., Reenan, R.A., and Graveley, B.R. (2004). Identification of alternative splicing regulators by RNA interference in Drosophila. Proc. Natl. Acad. Sci. USA *101*, 15974–15979.

Paz, I., Akerman, M., Dror, I., Kosti, I., and Mandel-Gutfreund, Y. (2010). SFmap: a web server for motif analysis and prediction of splicing factor binding sites. Nucleic Acids Res. *38*, W281–W285.

Pleiss, J.A., Whitworth, G.B., Bergkessel, M., and Guthrie, C. (2007). Transcript specificity in yeast pre-mRNA splicing revealed by mutations in core spliceosomal components. PLoS Biol. *5*, e90.

Porto, G., and De Sousa, M. (2007). Iron overload and immunity. World J. Gastroenterol. *13*, 4707–4715.

Ramm, G.A., and Ruddell, R.G. (2010). Iron homeostasis, hepatocellular injury, and fibrogenesis in hemochromatosis: the role of inflammation in a noninflammatory liver disease. Semin. Liver Dis. *30*, 271–287.

Rausin, G., Tillemans, V., Stankovic, N., Hanikenne, M., and Motte, P. (2010). Dynamic nucleocytoplasmic shuttling of an Arabidopsis SR splicing factor: role of the RNA-binding domains. Plant Physiol. *153*, 273–284.

Ray, D., Kazan, H., Cook, K.B., Weirauch, M.T., Najafabadi, H.S., Li, X., Gueroussov, S., Albu, M., Zheng, H., Yang, A., et al. (2013). A compendium of RNA-binding motifs for decoding gene regulation. Nature *499*, 172–177.

Roesler, J., Izquierdo, J.M., Ryser, M., Rösen-Wolff, A., Gahr, M., Valcarcel, J., Lenardo, M.J., and Zheng, L. (2005). Haploinsufficiency, rather than the effect of an excessive production of soluble CD95 (CD95DeltaTM), is the basis for ALPS Ia in a family with duplicated 3′ splice site AG in CD95 intron 5 on one allele. Blood *106*, 1652–1659.

Saltzman, A.L., Pan, Q., and Blencowe, B.J. (2011). Regulation of alternative splicing by the core spliceosomal machinery. Genes Dev. *25*, 373–384.

Sanchez, M., Galy, B., Schwanhaeusser, B., Blake, J., Bähr-Ivacevic, T., Benes, V., Selbach, M., Muckenthaler, M.U., and Hentze, M.W. (2011). Iron regulatory protein-1 and -2: transcriptome-wide definition of binding mRNAs and shaping of the cellular proteome by iron regulatory proteins. Blood *118*, e168–e179.

Solier, S., Lansiaux, A., Logette, E., Wu, J., Soret, J., Tazi, J., Bailly, C., Desoche, L., Solary, E., and Corcos, L. (2004). Topoisomerase I and II inhibitors control caspase-2 pre-messenger RNA splicing in human cells. Mol. Cancer Res. *2*, 53–61.

Solier, S., Barb, J., Zeeberg, B.R., Varma, S., Ryan, M.C., Kohn, K.W., Weinstein, J.N., Munson, P.J., and Pommier, Y. (2010). Genome-wide analysis of novel splice variants induced by topoisomerase I poisoning shows preferential occurrence in genes encoding splicing factors. Cancer Res. *70*, 8055–8065.

Soret, J., Gabut, M., Dupon, C., Kohlhagen, G., Stévenin, J., Pommier, Y., and Tazi, J. (2003). Altered serine/arginine-rich protein phosphorylation and exonic enhancer-dependent splicing in Mammalian cells lacking topoisomerase I. Cancer Res. *63*, 8203–8211.

Strässer, K., Masuda, S., Mason, P., Pfannstiel, J., Oppizzi, M., Rodriguez-Navarro, S., Rondón, A.G., Aguilera, A., Struhl, K., Reed, R., and Hurt, E. (2002). TREX is a conserved complex coupling transcription with messenger RNA export. Nature *417*, 304–308.

Wahl, M.C., Will, C.L., and Lührmann, R. (2009). The spliceosome: design principles of a dynamic RNP machine. Cell *136*, 701–718.

Warzecha, C.C., Sato, T.K., Nabet, B., Hogenesch, J.B., and Carstens, R.P. (2009). ESRP1 and ESRP2 are epithelial cell-type-specific regulators of FGFR2 splicing. Mol. Cell *33*, 591–601.

Zheng, S., Damoiseaux, R., Chen, L., and Black, D.L. (2013). A broadly applicable high-throughput screening strategy identifies new regulators of Dlg4 (Psd-95) alternative splicing. Genome Res. *23*, 998–1007.

Zhou, Z., Qiu, J., Liu, W., Zhou, Y., Plocinik, R.M., Li, H., Hu, Q., Ghosh, G., Adams, J.A., Rosenfeld, M.G., and Fu, X.D. (2012). The Akt-SRPK-SR axis constitutes a major pathway in transducing EGF signaling to regulate alternative splicing in the nucleus. Mol. Cell *47*, 422–433.